Oscillatory Bottom Boundary Layers

GEORGE MELLOR

Atmospheric and Oceanic Sciences Program, Princeton University, Princeton, New Jersey

(Manuscript received 31 July 2001, in final form 9 April 2002)

ABSTRACT

A turbulence closure model is applied to the case of an oscillating boundary layer; model calculations compare favorably with data. Wave-induced oscillations can be temporally resolved in a one-dimensional model but not in three-dimensional ocean models, and, indeed, statistical wave models, working in consort with ocean models, can only provide information on expected wave periods and amplitudes. Therefore, in this paper, a way has been found to parameterize the effects of bottom flow oscillations; it entails augmenting the turbulence shear production as a function of amplitude and period of the oscillation, the bottom shear stress of the mean current flow, and the angle between the directions of the oscillations and the mean flow. The more conventional method of solving for an apparent wall roughness is also investigated in an appendix.

1. Introduction

The influence of short-period, surface wave–induced oscillations on bottom boundary layers has commanded considerable attention in the literature since the pioneering studies of Grant and Madsen (1979). They presented a theory that embodied analyses and several assumptions including spatially linear and temporally constant eddy viscosities; as a result, the effect of the oscillations is parameterized as an enhanced surface roughness. This approach has been further refined by Grant and Madsen (1986, henceforth GM86; see appendix D), Glenn and Grant (1987), and Mathisen and Madsen (1996a,b). The latter authors introduced a correction to the Grant–Madsen theory to account for variability in the eddy viscosity. These theories are algebraically very complicated, but in principal, they could be used in numerical general ocean circulation modeling. Malarkey and Davies (1998) introduced a similar semianalytical theory with somewhat different assumptions. Hagatun and Eidsvik (1986) and Li and Davies (1996), using a $k - \epsilon$ model, calculated temporally resolved, one-dimensional, numerical simulations of combined mean current and oscillatory flow, this in conjunction with sediment transport modeling. Papers by Justesen (1991) and Brors and Eidsvik (1994) also successfully applied $k - \epsilon$ models to the data described below, and their papers are complimentary to this paper. These studies, while quite successful, did not provide information directly useful to general ocean circulation models where time steps are on the order of minutes to hours whereas, to resolve surface wave timescales, time steps are a small fraction of a second.

The purpose of this paper is to provide a means of parameterizing the effect of oscillations on an otherwise stationary or slowly varying mean flow, which can be incorporated in ocean models. The result is not much more complicated than that inherent in basic turbulence closure models, one of which is necessarily reviewed here and which involves the solution of the turbulence kinetic energy equation (TKE).

Consider a flow governed by

$$\frac{\partial u}{\partial t} = P_0 + P_1 \cos(\omega t) + \frac{\partial \tau}{\partial z}; \qquad (1a)$$

$u = u(z, t)$ is the ensemble mean velocity, t is time, and z is the distance from a solid surface located at $z = 0$ where $u = 0$. The Reynolds stress τ is taken to be a kinematic stress, that is the dynamic stress divided by the fluid density. This one-dimensional flow is driven by a kinematic, horizontal pressure gradient $P_0 + P_1 \cos(\omega t)$, which has spatially independent, steady and oscillatory components. We further specialize to flow in a channel whose height is $2h$. Because of symmetry, we need only solve for flow properties in the region, $0 \le z \le h$. The time average of a fully developed (a long time after forcing is initiated) flow is

$$P_0 = -\frac{\partial \overline{\tau}}{\partial z} = \frac{\overline{\tau}_0}{h}, \qquad (1b)$$

where $\overline{\tau}_0$ is the mean shear stress at $z = 0$ and, of course, $\overline{\tau} = 0$ at $z = h$.

For pure oscillatory flow, $P_0 = \overline{\tau}_0 = 0$, $P_1 > 0$, in which case the active boundary layer is typically con-

---

Corresponding author address: Dr. George Mellor, Atmospheric and Oceanic Sciences Program, Princeton University, Box CN710, Sayre Hall, Princeton, NJ 08544-0710.
E-mail: glm@splash.princeton.edu

© 2002 American Meteorological Society

fined to a thin region near the surface. This problem can be transformed to oscillating plate flow above which the flow is stationary, a problem that is termed a Rayleigh flow or Stokes second problem (Schlicting 1979). For laminar flow, the boundary layer thickness is $\delta_\omega \simeq 7\sqrt{\upsilon/\omega}$. For turbulent flow, approximate an eddy viscosity such that $\upsilon \propto u_{\tau m}\delta_\omega$ where $u_{\tau m}^2$ is an average wall shear stress, defined below. Thus, $\delta_\omega \simeq 1.2u_{\tau m}/\omega$ where the constant of proportionality is determined below. The velocity amplitude of the oscillations is $u_b = P_1\omega^{-1}$ and a more useful formula is $\delta_\omega \simeq 0.04u_b/\omega$ from which it can be shown that wave-induced, bottom boundary layer thicknesses in the ocean are quite small and of the order 10 cm.

For fully developed mean flow ($P_0 > 0$) superimposed on oscillatory flow ($P_1 > 0$), the conceptual model (Grant and Madsen 1979) is that the region near a (bottom) surface, influenced by the oscillations, is small as in the pure oscillatory case and directly affects the mean flow only in this small region. Indirectly, the mean outer flow behaves like a flow over a roughness enhanced surface.

2. The model

The so-called Mellor–Yamada (M–Y) model (Mellor and Yamada 1982, henceforth MY82; Mellor 2001) will be invoked to relate the shear stress to the velocity so that

$$\tau = K_M\frac{\partial u}{\partial z}, \tag{2a}$$

$$K_M \equiv S_{M0}ql, \tag{2b}$$

where $q^2/2$ is the turbulence kinetic energy and l is the master length scale. Generally, S_M is a function of a density stratification parameter, but here we specialize to neutral flow so that $S_M = S_{M0} = 0.39$. The model does not attempt to solve for properties into the viscous or roughness layer or inner layer; it numerically solves for properties in the outer layer and then matches this outer solution to empirically known inner functions. The inner and outer solutions for velocity have a common overlap layer, the well-known law of the wall, which is the inner asymptote (for small z) for the outer function and the outer asymptote for the inner function (for large z after appropriate rescaling; Mellor 1972). The overlap layer for q is simply a constant proportional to the square root of the shear stress at the wall (Perry and Abell 1975; MY82).

The important boundary conditions for (1) are that u is matched (see appendix A) to the law of the wall such that

$$u(z, t) = \frac{\tau_0(t)}{\kappa u_\tau(t)}\ln\left(\frac{z}{z_0}\right), \qquad z = z_{\mathrm{lw}}, \tag{3a}$$

where

$$u_\tau(t) \equiv |\tau_0(t)|^{1/2} \tag{3b}$$

and $\kappa = 0.4$ is von Kármán's constant; z_0 is the roughness parameter. For smooth surfaces, $z_0 = 0.141\upsilon/u_\tau$ (for water, $\upsilon = 1.14 \times 10^{-6}\ \mathrm{m^2\ s^{-1}}$) whereas for rough walls $z_0 = k/30$ where k is a measure of the actual wall roughness. Here z_{lw} represents any value greater than z_0 and much less than the outer dimension of the problem, in the present case, h. Equation (3) may be derived from (2a,b) where $\tau = \tau_0$ and the empirical findings that, in the law of the wall region, $q = u_\tau/S_{M0} = 2.56u_\tau$ (MY82) and $l = \kappa z$. Numerically, in our staggered grid arrangement, z_{lw} is set to its values at the midpoint between the bottom and the first grid level nearest the bottom.

The law of wall agrees with data only when $z/z_0 \gg 1$; this is easily seen in turbulent flow measurements close to a smooth wall, for example. Generally, $z_{\mathrm{lw}}/z_0 \gg 1$; however, there could arise cases of large z_0 whence the value of z_{lw} might be less than z_0 rendering (3a) invalid. Specifically, this would yield a negative logarithm in (3) prompting some to let $l = \kappa(z + z_0)$ in which case the logarithmic term in (3a) is replaced by $\ln(1 + z/z_0)$. This issue and the matching procedure are discussed further in appendixes A and B.

To provide $q(z, t)$, the turbulence kinetic energy is solved according to

$$\frac{\partial q^2}{\partial t} = \frac{\partial}{\partial z}\left(S_q ql\frac{\partial q^2}{\partial z}\right) + 2P_S - 2\frac{q^3}{B_1 l}. \tag{4}$$

The terms in (4) represent tendency, diffusion, shear production and dissipation, respectively. The shear production is given by

$$P_S = K_M\left(\frac{\partial u}{\partial z}\right)^2 \tag{5}$$

and will be modified in sections 4 and 5. Model constants are $B_1 = 16.6$ and $S_q = 0.20$. It may be shown that $S_{M0} = B_1^{-1/3} = 0.39$. The boundary conditions for (4) are $\partial q^2/\partial z = 0$ at $z = 0$ and $z = h$.

Finally, the master length scale equation is

$$\frac{\partial q^2 l}{\partial t} = \frac{\partial}{\partial z}\left(S_q ql\frac{\partial q^2 l}{\partial z}\right) + E_1 lP_S - \frac{q^3}{B_1}\left[1 + E_2\left(\frac{l}{\kappa L}\right)^2\right], \tag{6}$$

where $S_q = 0.2$, $E_1 = 1.8$, and $E_2 = 1.33$. For channel flow the ''wall proximity function'' L is given by

$$L^{-1} \equiv \frac{1}{(2h - z)} + \frac{1}{z}. \tag{7}$$

As discussed in MY82 and following Wolfshtein (1970), Eq. (6) is the two-point correlation function integrated with respect to the distance separating the two points. We have always acknowledged that (6) is the more empirical part of the model and, unlike the other constants, S_q, E_1, and E_2 were determined (MY82) by a best fit of calculations with both boundary layer (for which $h \to \infty$

so that $L = z$) and channel flow data and by the constraint, $l \sim \kappa z$ as $z \rightarrow 0$. The boundary conditions for (6) are that $\partial q^2 l/\partial z = 0$ at $z = h$ and $l = 0$ at $z = 0$.

In addition to (3b), we now define

$$u_{\tau m}^2 \equiv \overline{|\tau_0|} \quad \text{and} \tag{8a}$$

$$\overline{u}_\tau^2 \equiv |\overline{\tau}_0|, \tag{8b}$$

where the overbar represents a time average. Note that, for pure oscillatory flow, $\overline{u}_\tau = 0$ whereas $u_{\tau m} > 0$.

In MY82, Mellor (2001) and elsewhere, the model has been shown to have a large range of application; it has proven to be a quite general turbulence closure model. Relevant to this paper, the model reproduced data for stationary channel flow and unbounded boundary layer flow. Using the present algorithm, the channel flow case (not shown) has been repeated with results identical to that in MY82. Thus, there is good reason to believe that the model will work well for oscillatory flow and, if it does so, it is reasonable to assume that it can simulate data for mixed mean current and oscillatory flow.

3. The oscillatory flow data of Jensen et al.

The model will now be tested against pure oscillatory data obtained in the laboratory by Jensen et al. (1989). This study represents an ingenious experiment whereby water in a U-shaped channel with two straight vertical legs and a connecting horizontal test section was made to oscillate by imposition of oscillatory air pressure at the end of one of the vertical legs; the other end was open to the atmosphere. The oscillations were quite monochromatic and could, to good approximation, be represented by the pressure term in (1a). The test channel depth was 0.28 m so that $h = 0.14$ m. The width-to-depth ratio, the aspect ratio, was 1.39. This is not very large and one worries about side wall effects although the oscillatory boundary thickness is less than h. The length of the constant depth test section was 10 m.

Velocities were measured with a laser–Doppler velocimeter (LDV) and were sampled at 15° intervals over 80 cycles so that mean and turbulence variances were ensemble averaged. Since $u(\vartheta) = -u(180° + \vartheta)$, $\tau(\vartheta) = -\tau(180° + \vartheta)$, and $q^2(\vartheta) = q^2(180° + \vartheta)$, only data for $0 < \vartheta < 180°$ were recorded. The period of oscillation was 9.6 s; thus, $\vartheta = 360° \times t/9.6$ s. The data for the highest Reynolds number correspond to a centerline velocity amplitude of $u_b = 2$ m s^{-1}. In this pure oscillatory case, the stress term in (1a) at centerline is nil, so that $P_1 = \omega u_b$.

The model uses 50 grid points distributed with equal spacing except near the bottom where 8 of the grid points were distributed logarithmically; the lowest-velocity grid point was located at $0.18 \times 10^{-3}h$. The time step was 0.04 s. The model was run to cyclic equilibrium, which was established in about 10 cycles. The model was run for 25 cycles.

Figure 1 shows the cyclic mean velocity from the model compared with the data plotted in linear form, whereas Fig. 2 shows the same information semilogarithmically. The agreement between model and data is quite good. There is some phase difference near $\vartheta = 0°$. [A detailed comparison of $u(h, t)$ indicates that the forcing in (1) might possibly contain a second harmonic but not enough to warrant the concomitant complexity.] The dashed lines are from Eq. (3) using model values of τ_0 (t).

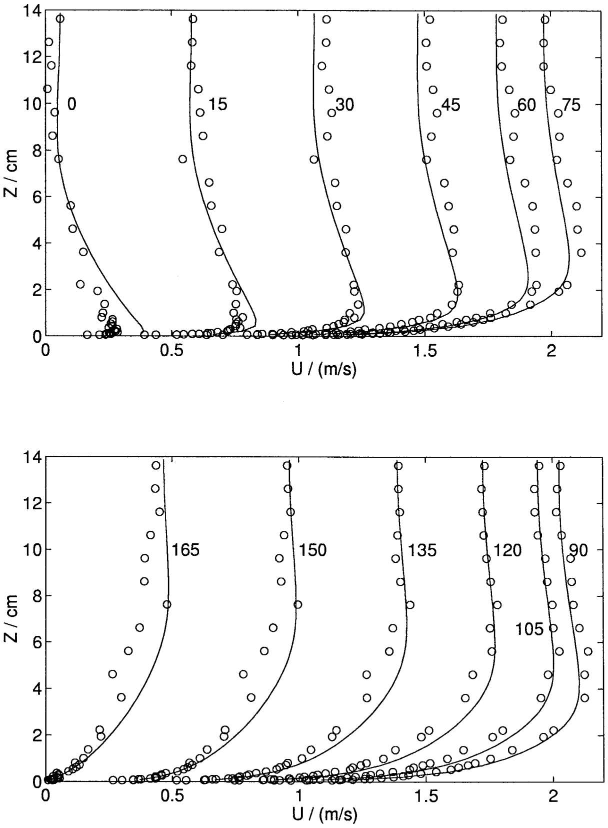

FIG. 1. Smooth wall velocity profiles for an oscillating flow over a smooth wall. Labels are phases in degrees; for 180° to 360°, the flow is a mirror image of those shown. The solid curves are calculated and the open circles are data from Jensen et al. (1989).

Figures 3 and 4 compare the Reynolds shear stress, τ, and twice the turbulence kinetic energy, q^2. A flush-mounted wall gauge measured the wall shear stress independent of the LDV-measured Reynolds stress, and these data are shown as the open squares in Fig. 3. This was an important measurement since the LDV measurements near the wall differed significantly from the wall gauge measurements. Measurements of the vertical component of q^2 were done separately and were scarce; however, they did not greatly differ from the cross-stream component so that we have set $q^2 = \overline{(u')^2} + 2\overline{(v')^2}$. The behavior of l is unremarkable; it behaves like κz for small z and then asymptotically approaches a constant 2.5 cm for large z.

Figure 5 is a comparison plot of the shear stress at

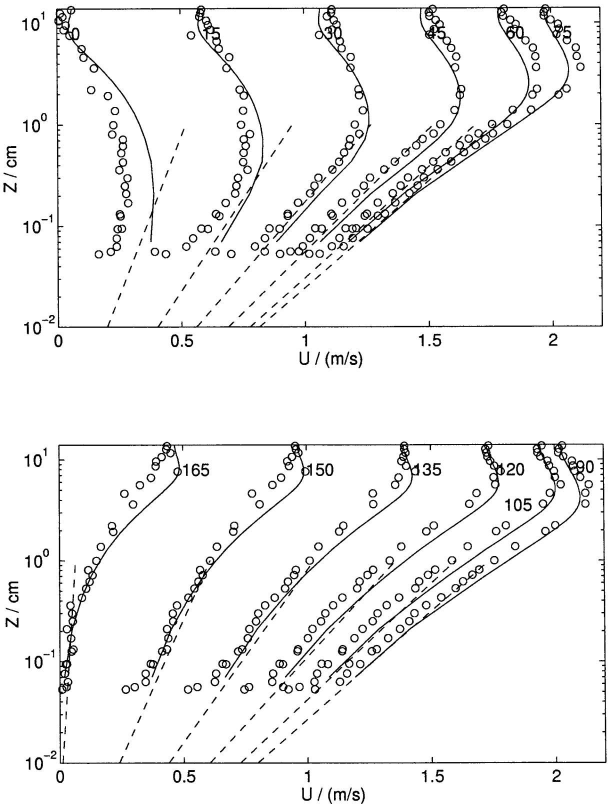

FIG. 2. Same as Fig. 1 but the vertical axis is logarithmically distributed. The dashed lines are according to Eq. (3).

the wall according to the model, the wall gauge measurements and results of matching Eq. (3) to the measured velocity data in the law-of-the-wall region (0.1 cm $< z <$ 0.9 cm). The zero stress point right around 165° is simulated quite well. It should be noted there is reason to believe that the law of the wall should not apply near the point where $\tau = 0$, but except for the near-wall profile for 0°, there is little evidence of this in Figs. 2 or 5.

The variance measurements for z less than 1 or 2 cm contain significant error since the LDV Reynolds stress measurements near the wall differ from both the wall gauge measurements and the stresses obtained from matching the cyclic mean velocity data with the law of the wall. This is presumably true of the q^2 measurements since, in the law of the wall region, $q^2/u_\tau^2 \simeq 6.5$. The variances also differ from the model when z is greater than about 4 cm. Variances, of course, are hard to measure, particularly in this oscillating environment. However, the fact that q^2 compares quite well with the data nearest 75° and 90° suggests these are data wherein the centerline slug of fluid moves least off the channel midpoint and that the other data may be influenced by the channel ends where the channel expands and then turns 90°; the closest approach to the channel ends are experienced by the fluid measured at the midpoint when $\omega t = 0°$ and 180°.

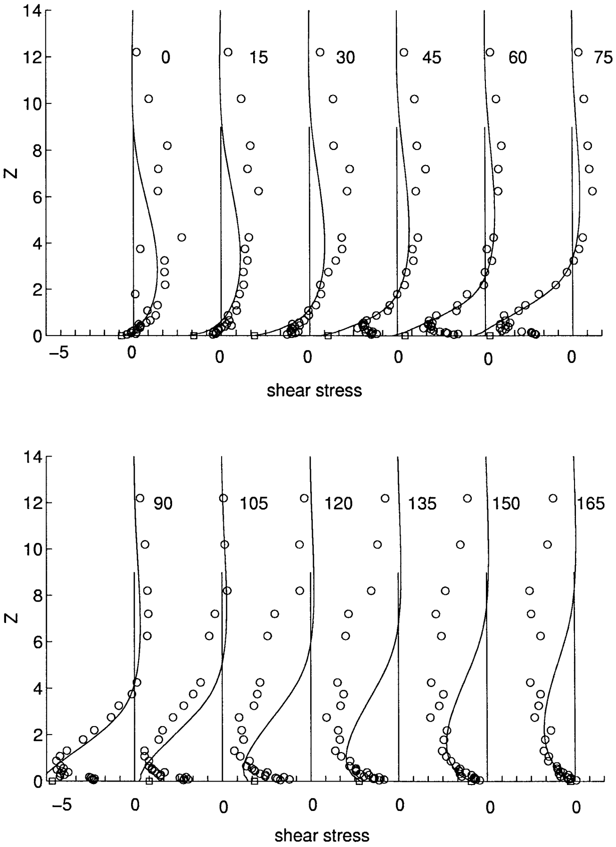

FIG. 3. Same as Fig. 1 but for the Reynolds shear stress; units are 10^{-3} m^2 s^{-2}. The open squares are measurements from a flush-mounted wall gauge.

Figure 6 includes plots of model–data comparisons of velocity in semilog coordinates for a rough wall where $k = 0.84$ mm so that $z_0 = 0.0028$ cm. The agreement of model and data near the wall is excellent. In the outer portions, there are some discrepancies. Figure 7 compares the model wall shear stress and the shear stress obtained by fitting the law of the wall to the measured velocity data in the region, 0.1 cm $< z <$ 0.9 cm. There were no wall gauge measurements in the rough wall case.

One must conclude that the model does a good job of simulating the experimental mean velocities and the wall shear stress. Otherwise, the LDV data and model variances sometimes agree and sometimes do not agree.

4. Mixed oscillatory and mean current flows

The general case of superimposed oscillatory and mean current is important to coastal oceanography, particularly if one adds the complication of sediment transport to the problem as described by Grant and Madsen (1979). In principle, the model, generalized for three-dimensional flow, could be used in ocean models such as the Princeton Ocean Model (POM; Blumberg and Mellor 1987; Mellor 1996); in fact, the turbulence clo-

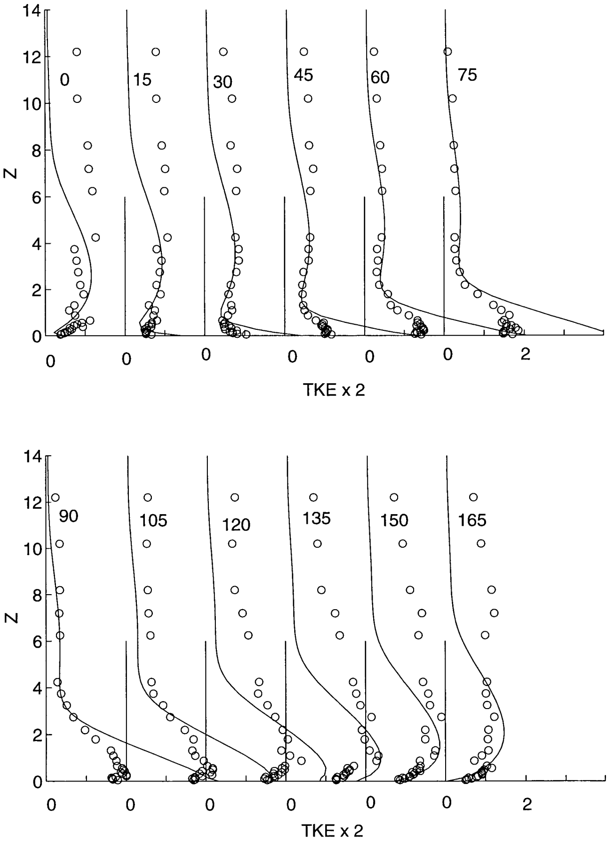

FIG. 4. Same as Fig. 1 but for twice the turbulence kinetic energy, q^2; units are 10^{-2} m^2 s^{-2}.

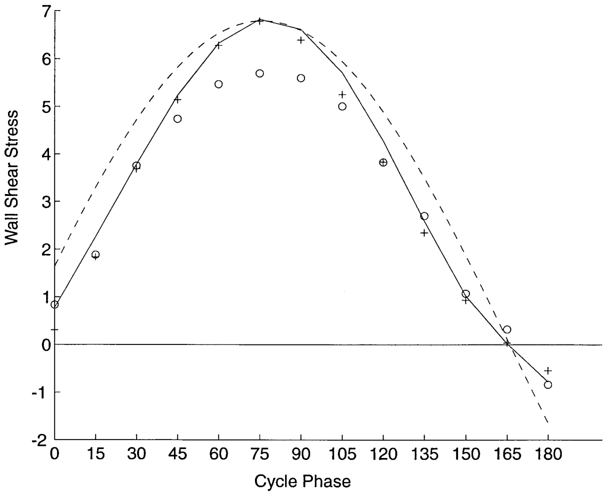

FIG. 5. The wall shear stress; units are 10^{-3} m^2 s^{-2}. The calculated values are the solid curve; the open circles are the wall gauge measurements and the crosses are determined by matching Eq. (3) to the velocity profile data for $z_0 = 0.141\upsilon/u_\tau$. A cosine curve (dashed) is added for reference; it is phase shifted so that its zero crossing agrees with the data and the calculations.

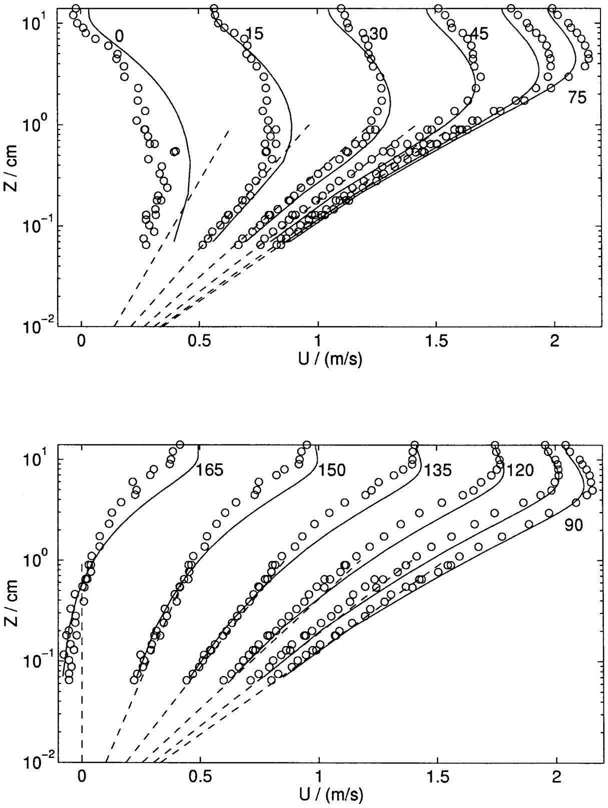

FIG. 6. Same as Fig. 2 but for a rough wall: $z_0 = 0.84/30$ mm.

sure model used here is a part of POM. However, such models cannot be run economically with the small time steps necessary to resolve wave induced oscillations with periods on the order of 10 s. Thus, it is necessary to parameterize the effects of the oscillations, and this

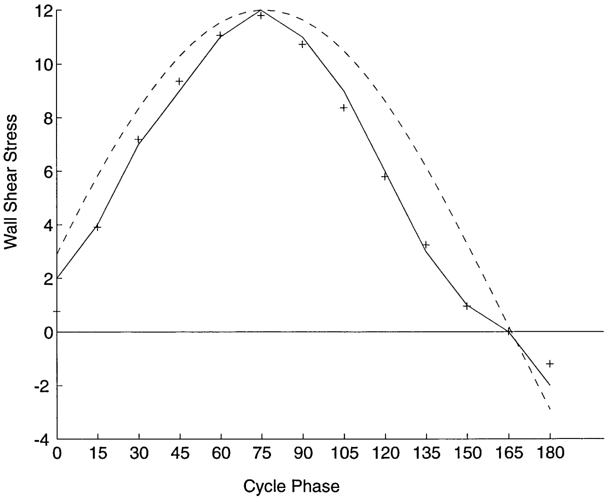

FIG. 7. Same as Fig. 5 but for a rough wall. There are no wall measurements and the crosses are determined by matching Eq. (3) to the velocity profile data for $z_0 = 0.84/30$ mm. A cosine curve (dashed) is added for reference.

will be the remaining goal of this paper for which we will compare calculations with the oscillations temporally resolved, as in section 3, with calculations where they are parameterized.

The momentum equations for the more general problem are

$$\frac{\partial u}{\partial t} = \frac{\overline{\tau}_{0x}}{h} + u_{bx}\omega \cos(\omega t) + \frac{\partial \tau_x}{\partial z}, \qquad (9a)$$

$$\frac{\partial v}{\partial t} = \frac{\overline{\tau}_{0y}}{h} + u_{by}\omega \cos(\omega t) + \frac{\partial \tau_y}{\partial z}, \qquad (9b)$$

where we directly introduce the important problem parameters: mean (kinematic) wall stress vector ($\overline{\tau}_{0x}$, $\overline{\tau}_{0y}$), and the velocity oscillatory amplitude vector (u_{bx}, u_{bx}). The only other modifications to the closure model are that (2a,b) becomes

$$(\tau_x, \tau_y) = K_M\left(\frac{\partial u}{\partial z}, \frac{\partial v}{\partial z}\right), \qquad (10a)$$

$$K_M = S_M q l \qquad (10b)$$

and (4b) becomes

$$P_S = K_M\left[\left(\frac{\partial u}{\partial z}\right)^2 + \left(\frac{\partial v}{\partial z}\right)^2\right]. \qquad (11)$$

Instead of (3), the model velocity near the wall is matched to

$$[u(z, t), v(z, t)] \sim \frac{[\tau_{0x}(t), \tau_{0y}(t)]}{\kappa u_\tau(t)} \ln\left(\frac{z}{z_0}\right), \qquad (12a)$$

$$z = z_{\mathrm{lw}}, \qquad (12b)$$

where

$$u_\tau^2 \equiv (\tau_{0x}^2 + \tau_{0y}^2)^{1/2}. \qquad (13)$$

It is convenient to continue numerically with the (laterally unbounded) channel flow problem as described by (9a,b), but since the effects of oscillations and their ultimate parameterization are confined to the near-wall region, we fully expect the latter to apply to boundary layers where (9a,b) might include advective terms or Ekman layers where Coriolis terms must be added to (9a,b). Although we will continue to deal with numerical simulations dimensionally, the final results must lean on dimensional analysis to reduce the parameters of the problem. Thus, for example, in the near-wall region, we expect the mean current velocities near a wall to be represented by

$$\overline{u} = \frac{\overline{\tau}_{0x}}{\overline{u}_\tau} f - \frac{\overline{\tau}_{0y}}{\overline{u}_\tau} g, \qquad (14a)$$

$$\overline{v} = \frac{\overline{\tau}_{0y}}{\overline{u}_\tau} f + \frac{\overline{\tau}_{0x}}{\overline{u}_\tau} g, \qquad (14b)$$

where the nondimensional profiles are

$$f = f\left(\frac{z\omega}{u_b}, \frac{\overline{u}_\tau}{u_b}, \phi, \frac{z_0\omega}{u_b}\right), \qquad (14c)$$

$$g = g\left(\frac{z\omega}{u_b}, \frac{\overline{u}_\tau}{u_b}, \phi, \frac{z_0\omega}{u_b}\right) \qquad (14d)$$

and where

$$\overline{u}_\tau^2 \equiv \overline{\tau}_0 \equiv (\overline{\tau}_{0x}^2 + \overline{\tau}_{0y}^2)^{1/2} \qquad (15a)$$

$$u_b \equiv (u_{bx}^2 + u_{by}^2)^{1/2}. \qquad (15b)$$

The angle ϕ between the oscillatory amplitude vector and the mean wall shear stress is given by

$$\sin\phi = \frac{|u_{by}\overline{\tau}_{0x} - u_{bx}\overline{\tau}_{0y}|}{u_b\overline{\tau}_0}. \qquad (15c)$$

In section 3, the data and model simulations were such that the oscillatory boundary layer almost filled the entire channel, roughly from $z = 0$ to 10 cm. Using the model as a tool, we will now explore the relationship between oscillatory and mean currents with $h = 2$ m. The value $h = 2$ m is much larger than the oscillatory influence depth δ_ω but still small enough to provide good numerical resolution. The parameter h is missing from (14) since, again, we do not expect the outer flow to influence the near surface flow. Because of the larger h and perhaps the inclusion of a mean current, the model was run for 500 cycles whence equilibrium was established.

In all of the numerical calculation performed below, we will set $\overline{\tau}_{0y} = 0$ so that (14a,b) simplifies to $\overline{u} = (\overline{\tau}_{0x}/\overline{u}_\tau) f$ and $\overline{v} = (\overline{\tau}_{0x}/\overline{u}_\tau) g$.

The model is first applied to the case where $\overline{\tau}_{0y} = u_{by} = 0$, $u_{bx} = 2$ m s^{-1}, and $\overline{\tau}_{0x} = 0.004$ m^2 s^{-2}. Also, set the oscillatory period to 9.6 s or $\omega = 0.654$ s^{-1}, a habit left over from section 3. The roughness is $z_0 = 3.06 \times 10^{-5}$ m so that $z_0\omega/u_b = 10^{-5}$. Thus, this is a flow where the oscillatory velocity component and the mean current component are collateral; that is, $\phi = 0°$. The time dependent velocity profiles are shown in Fig. 8 both in linear and semilogarithmic plots. The shear stresses are similarly shown in Fig. 9. For, say, $z \geq 30$ cm, the velocity shear and stress are not affected by the oscillatory flow near the wall.

Figure 10 shows time-averaged profiles in semilogarithmic coordinates for $\overline{\tau}_{0y} = 0$ and a range of values of $\overline{\tau}_{0x}$. Figure 10a shows cases where $u_{bx} = 2$, $u_{by} = 0$ m s^{-1} so that $\phi = 0°$; Fig. 10b demonstrates cases where $u_{bx} = u_{by} = \sqrt{2}$ m s^{-1} so that $\phi = 45°$; and Fig. 10c has cases where $u_{bx} = 0$, $u_{by} = 2$ m s^{-1} so that $\phi = 90°$. The dashed lines are law-of-the-wall plots from the phase-averaged Eq. (12a).

For both $\phi = 0$ and $\phi = 90°$, the function g of (14a,b) is identically zero, because of symmetry considerations, so that Figs. 10a and 10c, suitably nondimensionalized, yield the function f for $z_0\omega/u_b = 10^{-5}$. However, for intermediate values of ϕ, g is nonzero as seen in Fig.

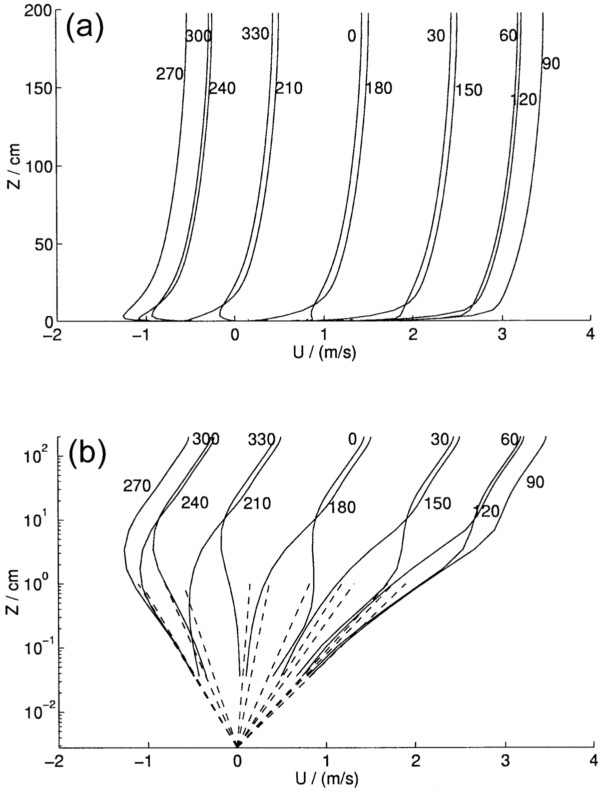

FIG. 8. Calculated profiles for a mixed mean current, $(\overline{\tau}_{0x}, \overline{\tau}_{0y}) = (0.004, 0)$ m^2 s^{-2} plus oscillatory flow $(u_b, v_b) = (2, 0)$ m s^{-1}, $\omega = 0.654$ s^{-1} on a rough wall $z_0 = 3.06 \times 10^{-5}$ m: (a) linear–linear plot, (b) log–linear plot. The dashed lines are from (12).

10b for $\phi = 45°$. This relates to the fact that the half cycle of the oscillation with a component in the direction of the mean current should behave differently than the half cycle opposite to the mean current. For $\overline{\tau}_{0y} = 0$, (9b) can be time-averaged and one obtains $\tau_{0y} = 0 = \overline{K}_M\, \partial\overline{v}/\partial z + \overline{K'_M \partial v'/\partial z}$, where the overbars are time averages and the primed quantities are deviations from the averages. For $0 < \phi < 90°$, the average of the deviatory terms are not zero and therefore neither is $\partial\overline{v}/\partial z$.

The function, g, while not zero, is fairly small, so in the interest of needed simplification, we shall henceforth assume that $g = 0$.

In Figs. 11a and 11b, the velocity profiles from Figs. 10a and 10c are repeated and are compared with mean current simulations with no oscillations; that is, $u_{bx} = u_{by} = 0$; these are the dashed curves. Thus Fig. 11 demonstrates error in stationary calculations if oscillations are present but neglected. The law-of-the-wall lines from (12a) are shortened here and fill the space, 0.03 cm $> z > z_0$.

Law-of-the-wall slopes

The problem now before us is to develop a way of parameterizing the stationary mean current calculations in order to eliminate much of the error shown in Fig. 11.

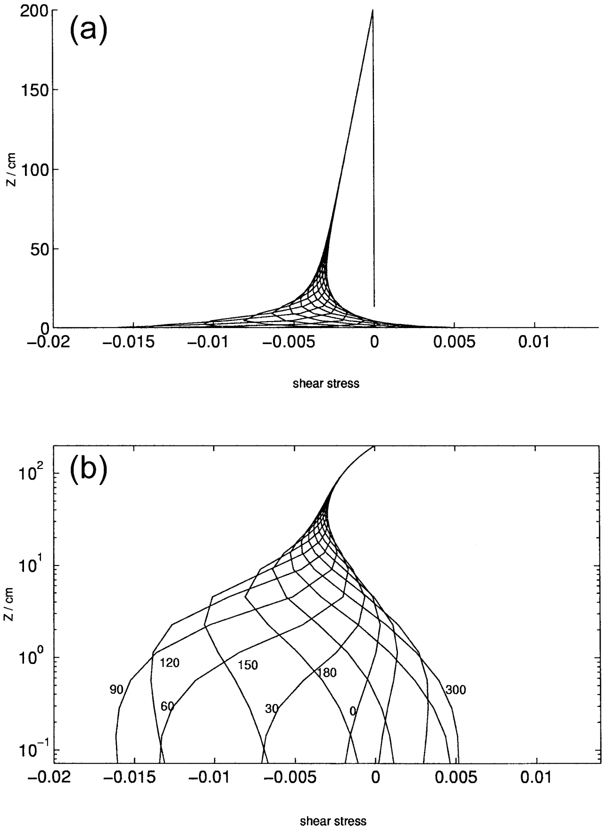

FIG. 9. Same as Fig. 8 but for the Reynolds shear stress; units are m^2 s^{-2}.

Before delving into this matter, we first explain why the oscillatory law-of-the-wall slopes differ from stationary slopes for the same mean wall stress. The explanation is fairly simple since the time average of (12a) is

$$\overline{u} = \frac{1}{\kappa}\overline{\left(\frac{\tau_{0x}}{u_\tau}\right)}\ln\left(\frac{z}{z_0}\right), \qquad \text{(16a)}$$

and therefore differs from the average of $\tau_{0x}(t)$ divided by the time average of $u_\tau(t)$ which is correct for mean (or slowly varying) current flow with no oscillations. Figure 12, corresponding to the profiles of Fig. 10, is a plot of the factor

$$\frac{\kappa\overline{u}_\tau z}{\overline{\tau}_{0x}}\frac{\partial\overline{u}}{\partial z} = \frac{\overline{(\tau_{0x}/u_\tau)}}{(\overline{\tau}_{0x}/\overline{u}_\tau)} \qquad \text{(16b)}$$

for $\phi = 0°$ (for which $\overline{\tau}_{0x}/\overline{u}_\tau = \overline{u}_\tau$), $\phi = 90°$, $z_0\omega/u_b = 10^{-5}$, and a range of values of $\overline{u}_\tau/u_b$. This plot is shown to emphasize the effect of oscillations on the log–law slope. That the nondimensional slope differs from unity is somewhat at odds with the practice of using the mean current value of $\overline{u}_\tau$ in the law of the wall but altering the roughness parameter z_0 to parameterize the effects of the oscillations. However, we will return to this subject in appendix D.

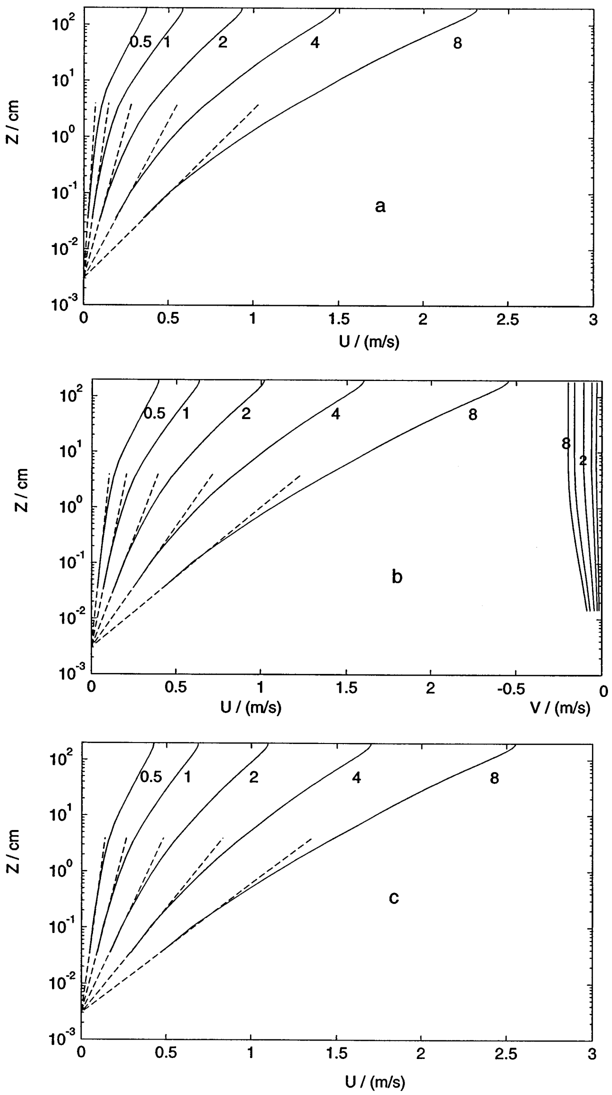

FIG. 10. Phase averaged profiles with the same parameters as Fig. 8 but for different values of $\overline{\tau}_{0x}$ and ϕ. The labels on the curves are $\overline{\tau}_{0x}$ with the units, 10^{-3} m^2 s^{-2}. The roughness parameter $z_0 = 3.06 \times 10^{-5}$ m and the oscillatory parameters are $\omega = 0.654$ s^{-1}: (a) (u_b, v_b) = (2, 0) m s^{-1} so that $\phi = 0$, (b) (u_b, v_b) = ($\sqrt{2}$, $\sqrt{2}$) m s^{-1} so that $\phi = 45°$, and (c) (u_b, v_b) = (0, 2) m s^{-1} so that $\phi = 90°$. The dashed lines are from the phase-averaged Eq. (12). In the case $\phi = 45°$, a cross current is generated that is fairly small and which henceforth will be neglected.

5. A procedure to parameterize the effects of oscillatory flow on the mean currents

The effects of oscillations on the mean current flow are felt through an increase in K_M, which is due to an increase in q, which in turn is due to an increase in shear production in Eq. (2a) or (10c). After some trial and error, a way has been found to approximate the effects of oscillatory flow without actually resolving the oscillations. The strategy is to add a term, P_A (apparent production), to the shear production in an otherwise stationary flow case. Thus,

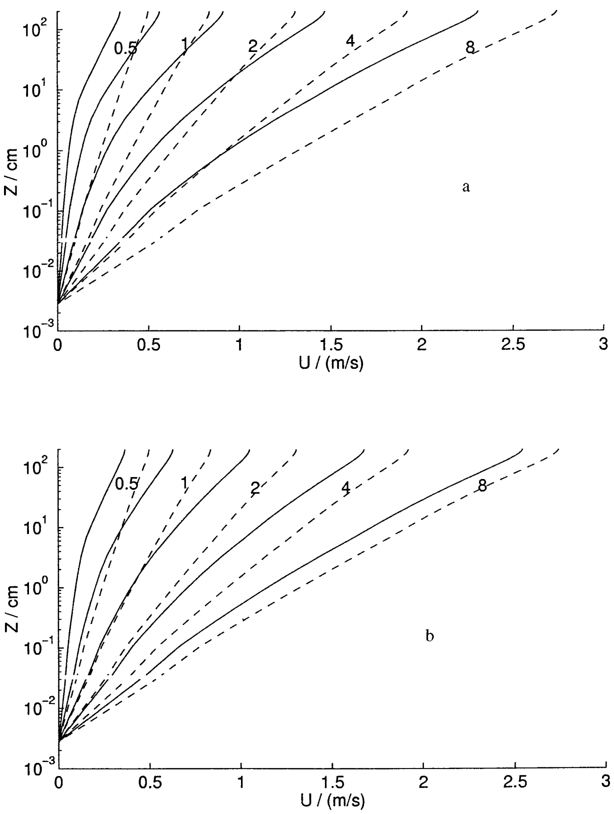

FIG. 11. The solid curves in (a) and (b) are repeated from Figs. 10a,c respectively, whereas the dashed curves are for the mean current alone, (u_b, v_b) = (0, 0). The differences between solid and dashed represent an error if oscillations exist but are neglected.

$$P_S = K_M\left[\left(\frac{\partial u}{\partial z}\right)^2 + \left(\frac{\partial v}{\partial z}\right)^2\right] + P_A. \tag{17}$$

Now the question is how to construct the function, P_A. First we note that

$$P_A/\omega u_b^2 = \text{fcn}(u_{\tau/u_b}, \phi, z_0\omega/u_b, z\omega/u_b).$$

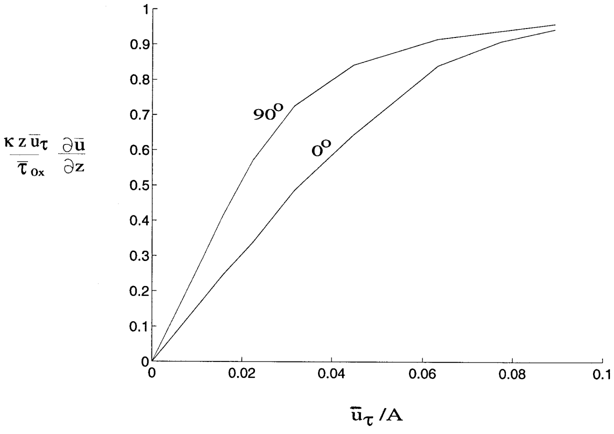

FIG. 12. The ratio of the phase-averaged law-of-the-wall slope to the slope obtained from the mean wall stress as expressed in (D1b).

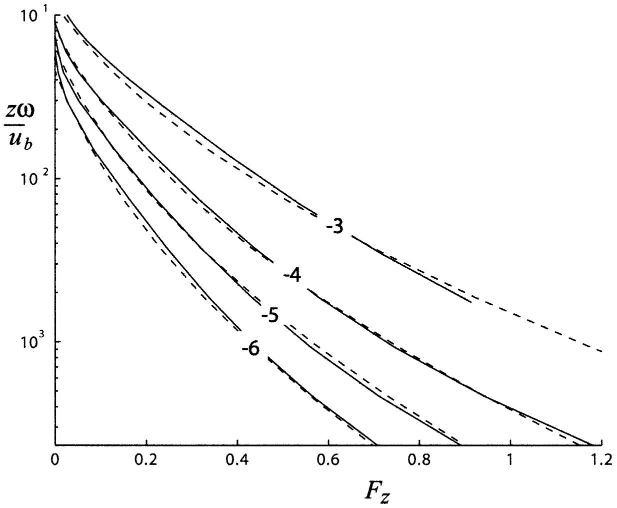

FIG. 13. The nondimensional production due to oscillations. The solid curves are obtained from numerous calculations where $\overline{\tau}_{0x}$ and z_0 are varied. The dashed curves are an approximate fit to the solid curves according to Eq. (21). The labels on each set of lines are values of $\log_{10}(z_0\omega/u_b)$; for the value -3, the vertical grid was altered so that the bottom-most grid point was greater than z_0.

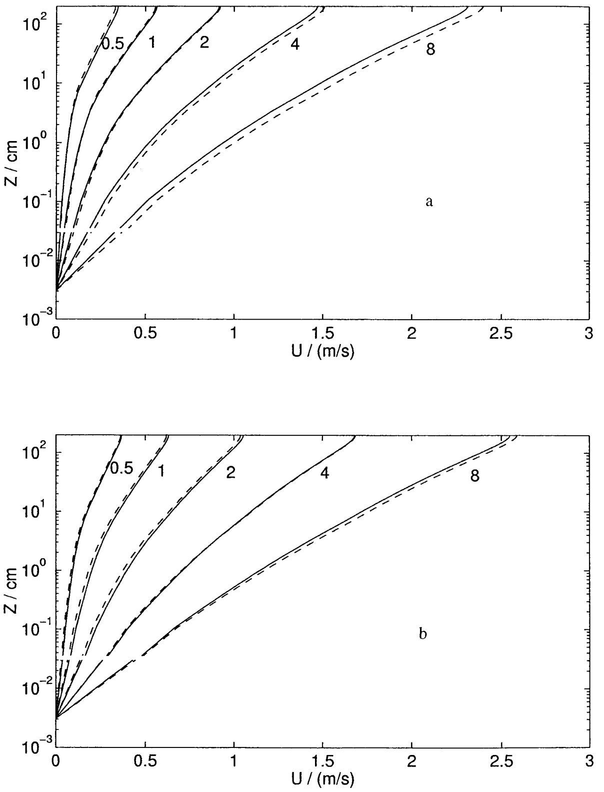

FIG. 14. A comparison of phase-averaged resolved solutions (solid curves) with the parameterized solutions (dashed curves) using Eqs. (9), (17), (18), (19), and (20). The labels on the curves are $\overline{\tau}_{0x}$ with the units, 10^{-3} m^2 s^{-2}. The oscillatory parameters are, $\omega = 0.654$ s^{-1} and $z_0 = 3.06 \times 10^{-5}$ m (a) $(u_b, v_b) = (2, 0)$ m s^{-1} so that $\phi = 0$; (b) $(u_b, v_b) = (0, 2)$ m s^{-1} so that $\phi = 90°$.

What we have found, surprisingly, and will shortly demonstrate, is that the sensitivity of the function to u_τ/u_b is negligible. Furthermore, the following separated form

$$\left(\frac{P_A}{\omega u_b^2}\right)^{1/3} = F_\phi(\phi)F_z\left(\frac{z\omega}{u_b}, \frac{z_0\omega}{u_b}\right) \tag{18}$$

is a good approximation. Here, F_z is obtained diagnostically from the phase averaged shear production from the pure oscillation cases for different values of z_0. A semilogarithmic plot of F_z is obtained from calculated oscillatory cases with no mean current flow and is shown as the solid curves in Fig. 13 for a three orders of magnitude spread in $z_0\omega/u_b$. The power, 1/3, introduces a convenience for numerical interpolation purposes, but physically it represents the fact that q is predominantly proportional to $P_S^{1/3}$ as discerned by inspection of (4), and it is the increase in q and therefore K_M that affects the calculated velocity profiles.

Before testing this procedure and before determining F_ϕ, it is necessary to modify the law of the wall since, with the added shear production, the relationship between q and u_τ in the law-of-the-wall region will change. Now, from (10a,b) and $l = \kappa z$, we obtain

$$(\overline{\tau}_{0x}, \overline{\tau}_{0y}) = \kappa S_{M0} z \overline{q}_0 \left(\frac{\partial \overline{u}}{\partial z}, \frac{\partial \overline{v}}{\partial z}\right),$$

which can be integrated while incorporating z_0 to obtain

$$(\overline{u}, \overline{v}) = \frac{(\overline{\tau}_{0x}, \overline{\tau}_{0y})}{\kappa S_{M0}\overline{q}_0} \ln\left(\frac{z}{z_0}\right), \qquad z = z_{\mathrm{lw}}, \tag{19}$$

where $\overline{q}_0$ is the value of $\overline{q}$ close to the wall. Actually, (19) is more general than the stationary form of (12a,b) and includes the standard situation when $P_A = 0$ and $S_{M0}q_0 = u_\tau$. Note that $\overline{q}_0$ is intrinsically positive definite, whereas the definition $\overline{u}_\tau = |\overline{\tau}_0|^{1/2}$ is a relatively complicated construct.

Calculations that include resolved oscillations are compared with parameterized calculations—using the phase averaged (9), (17), (18), and (19)—and are compared in Fig. 14a for the case $\phi = 0$; a best fit is obtained when $F_\phi = 1.44$. In Fig. 14b for the case, $\phi = 90°$, $F_\phi = 1.00$ is obtained. Further comparative calculations (not shown) for the intermediate values of $\phi = 22.5°$, 45.0°, 67.5° show that the parameterized profiles and the oscillation resolved profiles compare similarly to the 0° and 90° cases.

A straight-line fit for F_ϕ between $\phi = 0°$ and $\phi = 90°$ would be acceptable, but a better representation is

$$F_\phi = 1.22 + 0.22\cos(2\phi). \tag{20}$$

For ease of transportability, a curve fit (for $F_z > 0$; otherwise $F_z = 0$) is

$$\begin{aligned} F_z = {} & -0.0488 + 0.029\,17lz + 0.017\,03lz^2 \\ & + [1.125(lz_0 + 5) + 0.125(lz_0 + 5)^4] \\ & \times (-0.0102 - 0.002\,53lz + 0.002\,73lz^2), \end{aligned} \tag{21a}$$

where

$$lz \equiv \ln(z\omega/u_b) \quad \text{and} \tag{21b}$$

$$lz_0 \equiv \log_{10}(z_0\omega/u_b) \tag{21c}$$

and is shown in Fig. 13 as dashed curves.

Thus, to parameterize the effect of an oscillatory bottom boundary layer, one simply modifies the computer code that solves (17) and (19) and includes a subroutine that uses (18), (20), and (21) to deliver P_A as a function of u_b, ω, ϕ [provided by (15c) and wave amplitude components and wall stress components], and z_0.

6. Relation to the wave parameters

To use the results in ocean circulation models, wave parameters might be determined from wave climatologies or empirical wind related relations. Better yet, the ocean model should be wedded to a wave model.

For completeness we cite here the well-known wave relation. Presuming that the wave field can be approximated as a monochromatic wave with significant wave height H_s and dominant frequency σ_p, then

$$(u_{bx}, u_{by}) = 8^{-1/2}\frac{H_s g}{\sigma_p}\frac{(k_{px}, k_{py})}{\cosh kh}, \tag{22a}$$

$$\frac{\sigma_p h}{g} = k_p h \tanh k_p h, \tag{22b}$$

where k_p is the wavenumber, h is the water column depth, and the wave direction is specified by $(k_{px}, k_{py})/k_p$.

Conversely, the apparent shear production formulation, which here is input to the boundary layer submodel of the circulation model, is dissipation information for the wave energy equation (Komen et al. 1994). As discussed in appendix C, the wave dissipation is equal to $\omega u_b^2 F_z$ where F_z is given by (21). Spectral wave models require the vertically integrated dissipation; thus

$$D_w = \omega u_b^2 \int_{z_0}^{\delta_w} F_z^3\, dz, \tag{23}$$

where δ_ω bounds the region where $F_z > 0$.

After transforming from the linear z variable to a logarithmic variable, and then made dimensionless, the integration is carried out numerically to obtain

$$\begin{aligned}\log_{10}(z_0\omega/u_b,\ D_w/u_b^3) \\ = (-6,\ 0.000\,47,\ -5,\ 0.000\,95,\ -4,\ 0.001\,65, \\ -3,\ 0.003\,57)\end{aligned} \tag{24a}$$

or, approximately,

$$D_w = 0.029 \times 2^{\log_{10}(z_0\omega/u_b)}. \tag{24b}$$

7. Summary

In this paper, we first demonstrate that the M–Y turbulence closure model is capable of simulating the oscillating flow data of Jensen et al. (1989) as has been demonstrated in the past for other flows. The models of Justesen (1991) and Brors and Eidsvik (1994) did equally well in simulating the same data but were not advanced to the case of combined mean plus oscillating currents.

It is possible to temporally resolve the oscillations in a one-dimensional model but computationally impractical to do so in a three-dimensional ocean model. A new method has been determined to parameterize stationary calculations and the results have been compared with the resolved profiles. The method calls for the addition of a term to the shear production in the TKE equation while at the same time using the original roughness parameter in the law of the wall. The method is able to account for the effects of mean currents and the oscillatory parameters for a fairly large parameter space. A byproduct of this work is the determination of bottom wave dissipation for use in spectral wave models.

In appendix D, the method, wherein an apparent roughness parameter is used, is also determined as a function of mean currents and the oscillatory parameters; the results are compared with those obtained by the theory of GM86. The apparent roughness can be a couple of orders of magnitude larger than the actual roughness, a problem discussed in appendix B, and cannot describe the flow nearest the wall.

Although we have made reference to surface waves in this paper, the flow researched here lacks a free surface and there are no orbits and therefore no mean Stokes drift component of the mean flow; there is no ‘‘streaming flow’’ (Longuet-Higgins 1953), the effect of the bottom boundary layer in creating a wave Reynolds stress in addition to the conventional turbulence stress. Nevertheless, it is believed that the dissipation of oscillatory energy feeding into the turbulence kinetic energy equation, as quantified in this paper, should also apply to the interaction of surface waves and turbulent bottom boundary layers although there remain outstanding research questions.

Acknowledgments. This research was supported by the National Ocean Partnership Program. Thanks are due to Dr. B. M. Sumer for providing the data reported in Jensen et al. (1989) and to Dr. Alan Blumberg for commenting on a manuscript draft.

APPENDIX A

Wall Boundary Condition

The purpose of this appendix is to detail how the numerical velocity solutions are matched to

$$[u(z), v(z)] = \frac{(\tau_{0x}, \tau_{0y})}{\kappa S_{M0} q_0}\ln\left(\frac{z}{z_0}\right), \qquad z = z_{1/2}. \tag{A1}$$

In our basic model, the grid is arranged so that $z = 0$ and $k = 1$ is at the top of the ocean and $z = -H$ and

$k = kb$ is at the bottom. For this paper, where the bottom is the focus of attention and to simplify discussion, it was convenient to transpose the grid so that $z = 0$ and $k = 1$ denotes the bottom here and throughout the entire paper. The grid is staggered such that turbulence quantities are at the primary grid points, whereas the mean properties, u and v, are in the midpoints of these points. Thus $z_{1/2}$ is defined here as the velocity grid point, half a grid spacing from the bottom.

In POM and for the one-dimensional problem of this paper, the solution is split so that the horizontal pressure gradient, advective, diffusion terms and the Coriolis term are included according to $\tilde{u}_{k+1/2} - u^{n-1}_{k+1/2} = 2\Delta t \times$ (pressure gradient, etc.) and the vertical diffusion terms are included according to $u^{n+1}_{k+1/2} - \tilde{u}_{k+1/2} = 2\Delta t \times \partial\tau_x/\partial z$. Here n is the leapfrog time step and k is the vertical grid level. The step nearest the bottom may be discretized according to

$$u^{n+1}_{1/2} - \tilde{u}_{1/2} = \left(\frac{2\Delta t}{z_1 - 0}\right)\left(K_{M1}\frac{u^{n+1}_{3/2} - u^{n+1}_{1/2}}{z_{3/2} - z_{1/2}} - \tau_{0x}\right),$$

or, invoking (A1),

$$u^{n+1}_{1/2} - \tilde{u}_{1/2} = \left(\frac{2\Delta t}{z_1 - 0}\right)\left[K_{M1}\frac{u^{n+1}_{3/2} - u^{n+1}_{1/2}}{z_{3/2} - z_{1/2}} - \frac{u^{n+1}_{1/2}}{\kappa S_{M0} q_0 \ln(z_{1/2}/z_0)}\right]. \tag{A2}$$

This implicitly relates $u^{n+1}_{3/2}$ to $u^{n+1}_{1/2}$ and constitutes the lower boundary condition to our problem and incorporates the roughness parameter, z_0. Further numerical details can be found in Blumberg and Mellor (1987) and Mellor (1996).

APPENDIX B

Consequences of the Smallness of the Ratio $z_{1/2}/z_0$

If $z_{1/2}/z_0$ is less than unity then its logarithm is negative and one might suspect numerical difficulty. We have run stationary calculations ($u_b = 0$) for a range of τ_0 and found instabilities (the solutions would randomly vary in time but never completely diverge), independent of τ_0 when $z_{1/2}/z_0 < 0.8$ and stable solutions for $z_{1/2}/z_0 > 0.9$. We did not deem it important to refine the stability threshold, so we will say that the threshold was $z_{1/2}/z_0 \simeq 0.85$. This result was obtained without logarithmically distributed bottom points. When the log points were inserted at the bottom the threshold was reduced to $z_{1/2}/z_0 \simeq 0.4$. The fact that the threshold is not unity is somewhat curious but that is the finding. However, in practice, the difference between the exact threshold and unity is not important. Note that this discussion applies whether z_0 is that of sections 4 and 5 or the z_{0a} of appendix D; the latter, however, can be quite large. (Note also that solutions may behave numerically for $z_{1/2}/z_0 > 1$ but the solutions can not be assumed to be physically correct unless the ratio is large.)

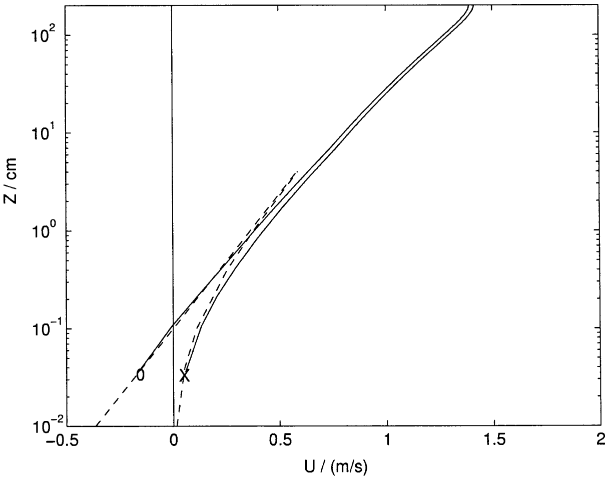

FIG. B1. A comparison of stationary profiles using two forms of the law of the wall, Eqs. (A1) (upper curve) and (B1) (lower curve): $z_{1/2} = 0.04$ cm and $z_0 = 0.1$ cm; $\overline{\tau}_{0x} = 0.004$ m^2 s^{-2}. Note that $z_{1/2}/z_0 = 0.4$; lesser values would be unstable using (A1) but stable using (B1).

One can avoid instability by simple redefining (A1) so that

$$[u(z),\ v(z)] = \frac{(\tau_{0x},\ \tau_{0y})}{\kappa S_{M0} q_0} \ln\left(\frac{z}{z_0} + 1\right), \qquad z = z_{1/2}. \tag{B1}$$

The log term behaves like $\ln(z/z_0)$ for large z/z_0, but asymptotically approaches z/z_0 for small z/z_0 so that the function is always positive. Together with (B1), the model must be slightly altered so that $K_M \equiv S_{M0}q(l + \kappa z_0)$, leaving the determination of l unchanged. Figure B1 compares a calculation using (A1) and the unaltered K_M with a calculation using (B1) and the altered K_M; both cases have logarithmically distributed grid points near the bottom. The difference between the two calculations is small so the alterations in K_M and (B1) would seem to represent a good numerical strategy to avoid instability. We did not invoke it in the main part of the paper because there is some virtue in having z_0 clearly represented as the $u = 0$ intercept in many of the plots.

APPENDIX C

Comments on Averaging

a. Mean currents

If we decompose K_M, u, and v into their time averaged parts denoted by overbar and the remainder oscillatory denoted by primes, then from (9a,b)

$$\overline{\tau}_x = \overline{\tau}_{0x}\left(1 - \frac{z}{h}\right) = \overline{K}_M \frac{\partial \overline{u}}{\partial z} + \overline{K'_M \frac{\partial u'}{\partial z}}, \qquad \text{(C1a)}$$

$$\overline{\tau}_y = 0 = \overline{K}_M \frac{\partial \overline{v}}{\partial z} + \overline{K'_M \frac{\partial v'}{\partial z}}, \qquad \text{(C1b)}$$

where we continue to align the coordinate system so that $\overline{\tau}_{0x} \geq 0$ and $\overline{\tau}_{0y} = 0$. By adding P_A to the shear production term in (17), we have in effect created a parameterized K_M, call it K_{MP}, to yield very nearly the same stationary $\partial\overline{u}/\partial z$ as in the resolved oscillatory solution. Thus, from (C1a)

$$K_{MP} = \overline{K}_M\left(1 + \frac{\overline{K'_M \partial u'/\partial z}}{\overline{K}_M \partial \overline{u}/\partial z}\right). \qquad \text{(C2)}$$

We have found that the factor in the square brackets is very nearly $F_\phi = 1.44$ when $\phi = 0°$ and must be identically 1.0 when $\phi = 90°$; thus, a partial explanation of the behavior of Eq. (20). From (C1b), it can be seen that $\partial\overline{v}/\partial z = \overline{K'_M \partial v'/\partial z} = 0$ when $\phi = 0°$ and $\phi = 90°$, otherwise $\partial\overline{v}/\partial z > 0$ as shown in Fig. 10.

b. Mean dissipation

The total dissipation (equal to the turbulence production) is

$$D = \overline{\tau}_x\left(\frac{\partial \overline{u}}{\partial z}\right) + \overline{\tau'_x\left(\frac{\partial u'}{\partial z}\right)} + \overline{\tau'_y\left(\frac{\partial v'}{\partial z}\right)}. \qquad \text{(C3)}$$

Evidently, the dissipation of the wave portion is

$$D_w = \overline{\tau'_x\left(\frac{\partial u'}{\partial z}\right)} + \overline{\tau'_y\left(\frac{\partial v'}{\partial z}\right)}. \qquad \text{(C4)}$$

We have made independent calculations of D_w [actually D and then $\overline{\tau}_x(\partial\overline{u}/\partial z)$ is subtracted] and found negligible differences between these calculations and F_z for a range of values of ϕ and $\overline{u}_\tau/u_b$.

APPENDIX D

The Apparent Roughness: Present Results Compared with the Grant–Madsen Model

It is now almost conventional to account for the effects of oscillatory bottom boundary layers by replacing z_0 with an apparent roughness parameter z_{0a}. This may be a necessary approach if one's boundary layer algorithm is an eddy viscosity approach [in which case reinstate $S_{M0}q_0$ with u_τ in (19a,b)] and therefore does not invoke a TKE equation.

The ratio z_{0a}/z_0 is given by

$$\frac{z_{0a}}{z_0} - 1 = F\left(\frac{\overline{u}_\tau}{u_b}, \phi, \frac{z_0\omega}{u_b}\right),$$

where F should vanish as $u_b/\overline{u}_\tau$ approaches zero. Since we are able to calculate temporally resolved oscillatory boundary layers (e.g., Fig. 10), we can match the conventional law of the wall to the phase averages of these calculations. An algorithm was created to determine z_{0a} for the average of 90 resolved oscillating profiles so that (21) could be evaluated. The results are shown in Fig. D1a in log–log form.

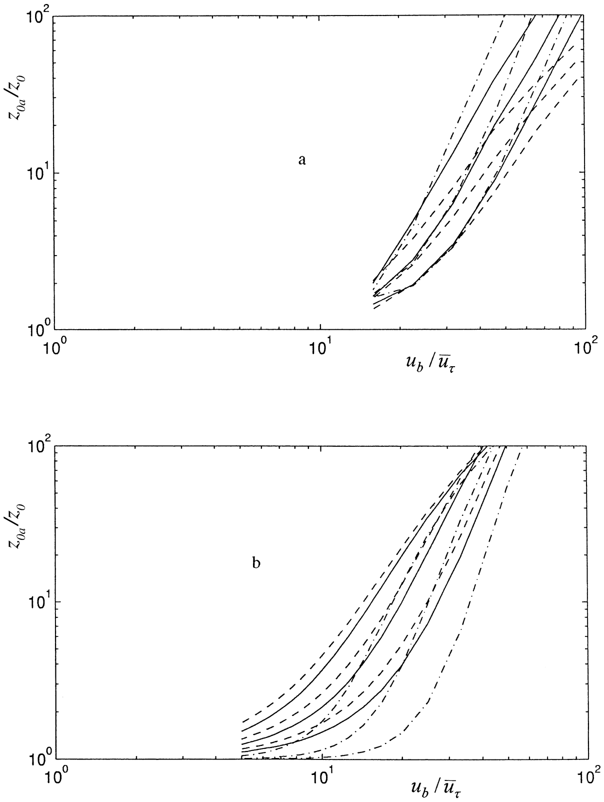

FIG. D1. (a) The apparent roughness to actual roughness ratio, z_{0a}/z_0, as a function of $u_b/\overline{u}_\tau$ and the values, $z_0\omega/u_b = 10^{-4}$ (dashed lines), 10^{-5} (solid lines), and 10^{-6} (dot–dashed lines). Within each $z_0\omega/u_b$ class, the three top-to-bottom curves are for $\phi = 0°, 45°, 90°$, respectively. (b) The apparent roughness–to–actual roughness ratio z_{0a}/z_0 from the theory of GM86.

Figure D2 is a comparison of the resolved solutions (solid curves), and the parameterized solutions (dashed curves) wherein the profiles are matched to the conventional law of the wall using the z_{0a} in Fig. D1a. The corresponding laws of the wall are shown as straight lines which intersect the $u = 0$ ordinate. They do indeed closely approximate the resolved solutions. The problem is that a good deal of the solution for small z is not available; this might be important to the sediment transport problem, for example. Furthermore, the calculations can be unstable if the matching point, z, is less than z_{0a}, which can be two or more orders of magnitude greater than z_0. In fact, for the calculations of Fig. D1a, the logarithmically distributed grid points near the bottom were eliminated so that the velocity grid point nearest the bottom is 10^{-2} h and always greater than z_{0a},

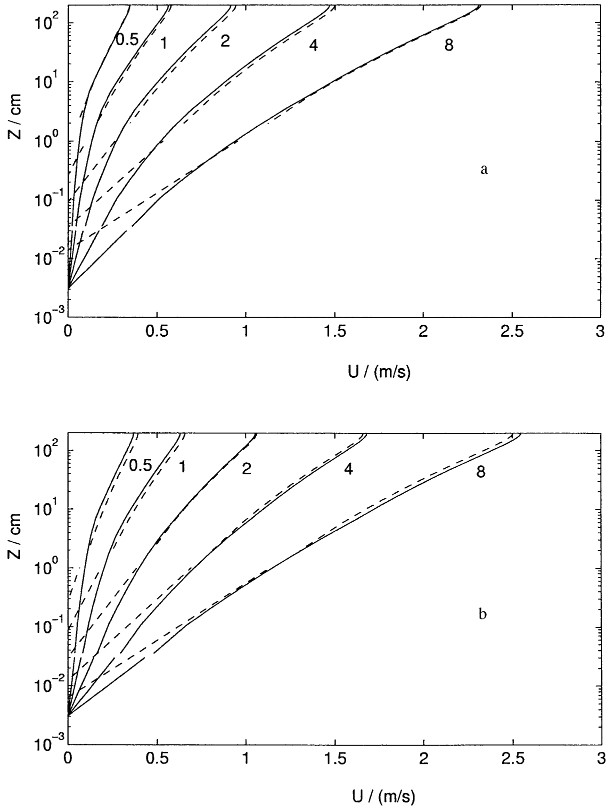

FIG. D2. A comparison of phase-averaged resolved solutions (solid curves) with the parameterized solutions (dashed curves) using Eq. (23) and the resulting apparent roughness in the law-of-the-wall matching condition from Fig. D1a. The labels on the curves are $\overline{\tau}_{0x}$ with the units, 10^{-3} m^{2} s^{-2}. The oscillatory parameters are $\omega = 0.654$ s^{-1} and $z_0 = 3.06 \times 10^{-5}$ m: (a) $\phi = 0°$, (b) $\phi = 90°$. The short straight lines (solid) and the longer lines (dashed) are law-of-the-wall plots where z_0 and z_{0a}, respectively, are denoted by the $u = 0$ intercepts.

thus avoiding an instability. This instability problem is researched in appendix B.

Next we compare the above results with results from the well-known Grant–Madsen model as we understand the model.

There are some details in Grant and Madsen (1979) that have been superseded (O. Madsen 2001, personal communication) by Grant and Madsen (GM86); the latter is therefore the basis of this summary unless otherwise stated.

Two boundary layer regions are defined such that

$$\tau_c = \kappa u_{*\mathrm{cw}} z(\partial u/\partial z) \quad \text{so that} \tag{D1a}$$

$$u(z) = \tau_c/(\kappa u_{*\mathrm{cw}}) \ln(z/z_0) \quad \text{for } z < \delta_{\mathrm{cw}} \tag{D1b}$$

$$\tau_c = \kappa u_{*\mathrm{c}} z(\partial u/\partial z) \quad \text{so that} \tag{D2a}$$

$$u(z) = \tau_c/(\kappa u_{*\mathrm{c}}) \ln(z/z_{0a}) \quad \text{for } z > \delta_{\mathrm{cw}}, \tag{D2b}$$

where u is the phase averaged current. Near the wall $z < \delta_{\mathrm{cw}}$, the eddy viscosity $\kappa u_{*\mathrm{cw}} z$ is characteristic of flow with a mean current plus an oscillating current. The roughness parmeter, z_0, equals $k_s/30$ where k_s is the Nikuradse equivalent roughness and therefore k_s or z_0 represents the actual wall conditions. Far from the wall $z > \delta_{\mathrm{cw}}$, the flow is governed by the conventional eddy viscosity $\kappa u_{*\mathrm{c}} z$, but with a boundary condition that uses an *apparent* roughness parameter z_{0a}, greater than z_0 due to the underlying oscillatory flow. In both cases τ_c is the mean shear stress in both law-of-the-wall regions and $u_{*\mathrm{c}}^2 = \tau_c$. (In this appendix we generally adhere to GM86 nomenclature but notice that $\overline{u}_\tau \equiv u_{*\mathrm{c}}$.)

GM86 is a theory to provide $u_{*\mathrm{cw}}^2$ and z_{0a}. Thus if we match the velocities from (D1b) and (D2b) at $z = \delta_{\mathrm{cw}}$ we obtain, after some manipulation, that

$$\frac{z_{0a}}{z_0} = \left(\frac{\delta_{\mathrm{cw}}}{z_0}\right)^{1-\epsilon}, \tag{D3a}$$

$$\epsilon \equiv \frac{u_{*\mathrm{c}}}{u_{*\mathrm{cw}}}. \tag{D3b}$$

For pure oscillatory flow, it is known that that $\delta_w \propto u_b/\omega$ where u_b is the orbital (but rectilinear) velocity near the wall. For mixed oscillatory, mean current flow, two assumptions are made. First,

$$\delta_{\mathrm{cw}} \equiv 2\kappa u_{*\mathrm{cw}}/\omega, \tag{D4}$$

and second

$$u_{*\mathrm{cw}}^2 = u_{*\mathrm{wm}}^2 C_R, \tag{D5a}$$

$$C_R \equiv \left[1 + 2\left(\frac{u_{*\mathrm{c}}}{u}\right)^2 \cos\phi + \left(\frac{u_{*\mathrm{c}}}{u}\right)^4\right]^{1/2}, \tag{D5b}$$

where $u_{*\mathrm{mw}}^2$ is the maximum friction velocity due to the oscillatory flow and

$$u_{*\mathrm{mw}}^2 = \frac{f_w}{2} u_b^2, \tag{D6}$$

where f_w is a friction factor for wave-induced oscillatory flow and u_b is the near-bottom wave velocity. [In GM86 a factor, $\sqrt{C_R}$, was erroneously included on the right side of (3) and then an adjustment was apparently made in a subsequent definition of f_w; O. Madsen 2001, personal communication.]

Doing the algebra, the above results may be written

$$\frac{z_{0a}}{z_0} \equiv \left(2\kappa \frac{u_{*\mathrm{cw}}}{u_b} \frac{u_b}{\omega z_0}\right)^{1-\epsilon}. \tag{D7}$$

There are several prescriptions for f_w in the literature, one in GM86 (which I could not reproduce algebraically), a curve (dashed line in Fig. 4) in Mathisen and Madsen (1996a) for which a curve fit (courtesy of Hydroqual Inc. and attributed to W. D. Grant) is

$$f_w = 0.23(A_b/k_s)^{-0.62}, \qquad A_b/k_s \le 12.5;$$

$$f_w = 0.13(A_b/k_s)^{-0.40}, \qquad A_b/k_s > 12.5, \tag{D8}$$

where $A_b \equiv u_b/\omega$ and one by Soulsby et al. (1993, where other relevant papers are cited), which is a curve fit of a fair amount of data for pure oscillatory flow; thus,

$$f_w = 0.3, \qquad A_b/k_s \leq 1.57;$$
$$f_w = 0.002\,51 \exp[5.21(A_b/k_s)^{-0.19}], \qquad k_s/A_b > 1.57. \tag{D9}$$

In and around midrange, $A_b/k_s \approx 1000$, the two formulations are in close agreement. Where they depart at high or low values, (D8) agrees somewhat better than (D9) with the data in Soulsby et al. and does not require the cutoff on the left side of (D9), which prevents otherwise unreasonably large values of f_w for small A_b/k_s. We therefore have used (D8) in the ensuing calculations from the GM86 theory.

For a fixed value of $A_b/k_s = 30^{-1}u_b/(\omega z_0)$, f_w is obtained from (D8). Then for an fixed ϕ and a range of values of $\overline{u}_\tau/u_b = u_{*\mathrm{c}}/u_b$, $u_{*\mathrm{cw}}/u_b$ can be obtained iteratively from (D5a,b) and (D6) converging on an asymptotic C_R. (For $\phi = 0°$ the equation set is considerably simplified and the iteration avoided.) Then values of z_{0a}/z_0 are obtained from (D3b) and (D7) and are plotted in Fig. D1b, which can be compared with Fig. D1a. Generally, the curves in Fig. D1a are shifted to the right and are more compact (less dependent on $z_0\omega/u_b$) relative to those in Fig. D1b.

REFERENCES

Blumberg, A. F., and G. L. Mellor, 1987: A description of a three-dimensional coastal ocean circulation model. *Three Dimensional Coastal Ocean Models,* N. Heaps, Ed., Coastal and Estuarine Sciences, Vol. 4, Amer. Geophys. Union, 1–16.

Brors, B., and K. J. Eidsvik, 1994: Oscillatory boundary layer flows modelled with dynamic Reynolds stress turbulence closure. *Cont. Shelf Res.,* **14,** 1455–1475.

Glenn, S. M., and W. D. Grant, 1987: A suspended sediment correction for combined wave and current flows. *J. Geophys. Res.,* **92,** 8244–8246.

Grant, W. D., and O. S. Madsen, 1979: Combined wave and current interaction with a rough bottom. *J. Geophys. Res.,* **84,** 1797–1808.

——, and ——, 1986: The continental-shelf bottom boundary layer. *Annu. Rev. Fluid Mech.,* **18,** 265–305.

Hagatun, K., and K. J. Eidsvik, 1986: Oscillating turbulent boundary layer with suspended sediments. *J. Geophys. Res.,* **91,** 13 045–13 055.

Jensen, B. L., B. M. Summer, and J. Fredsøe, 1989: Turbulent oscillatory boundary layers at high Reynolds numbers. *J. Fluid Mech.,* **206,** 265–297.

Justesen, P., 1991: A note on turbulence calculations in the wave boundary layer. *J. Hydraul. Res.,* **29,** 699–711.

Komen, G. J., L. Cavaleri, M. Donelan, K. Hasselmann, S. Hasselman, and P. A. E. M. Janssen, 1994: *Dynamics and Modelling of Ocean Waves.* Cambridge University Press, 532 pp.

Li, Z., and A. G. Davies, 1996: Towards predicting sediment transport in combined wave–current flow. *J. Waterw. Port Coastal Ocean Eng.,* **122,** 157–164.

Longuet-Higgins, M. S., 1953: Mass transport in water waves. *Philos. Trans. Roy. Soc. London,* **245A,** 535–581.

Malarkey, J., and A. G. Davies, 1998: Modelling wave–current interaction in rough turbulent bottom boundary layers. *Ocean Eng.,* **25,** 119–141.

Mathisen, P. P., and O. S. Madsen, 1996a: Waves and currents over a fixed rippled bed. 1. Bottom and apparent roughness experienced by currents in the presence of waves. *J. Geophys. Res.,* **101,** 16 533–16 542.

——, and ——, 1996b: Waves and currents over a fixed rippled bed. 2. Bottom roughness experienced by waves in the presence and absence of currents. *J. Geophys. Res.,* **101,** 16 543–16 550.

Mellor, G. L., 1972: The large Reynolds number asymptotic theory of turbulent boundary layers. *Int. J. Eng. Sci.,* **11,** 851–873.

——, 1996: Users guide for a three-dimensional primitive equation numerical ocean model. Princeton University Rep., Program in Atmospheric and Oceanic Sciences, Princeton University, Princeton, NJ, 41 pp. [Available online at www.aos.princeton.edu/wwwpublic/htdocs.pom/.]

——, 2001: One-dimensional, ocean surface layer modeling: A problem and a solution. *J. Phys. Oceanogr.,* **31,** 790–809.

——, and T. Yamada, 1982: Development of a turbulence closure model for geophysical fluid problems. *Rev. Geophys. Space Phys.,* **20,** 851–875.

Perry, A. E., and C. J. Abell, 1975: Scaling laws for pipe-flow turbulence. *J. Fluid Mech.,* **67,** 257–271.

Schlicting, H., 1979: *Boundary Layer Theory.* McGraw-Hill, 817 pp.

Soulsby, R. L., L. Hamm, G. Klopman, D. Myrhaug, R. R. Simons, and G. P. Thomas, 1993: Wave–current interaction within and outside the bottom boundary layer. *Coastal Eng.,* **21,** 41–69.

Wolfshtein, M., 1970: On the length-scale-of-turbulence equation. *Is. J. Technol.,* **8,** 87–99.